Study of plant fibre composites with damage induced by laser and mechanical impacts

Paweł H. Malinowski[a,*], Wiesław M. Ostachowicz[a], Fabienne Touchard[b], Michel Boustie[b], Laurence Chocinski-Arnault[b], Pedro Pascual Gonzalez[b], Laurent Berthe[c], Davi Silva de Vasconcellos[d], Luigi Sorrentino[d]

[a] *Institute of Fluid–Flow Machinery, Polish Academy of Sciences, Fiszera 14, 80–231, Gdansk, Poland*
[b] *Institut PPRIME, CNRS, ISAE-ENSMA, Université de Poitiers, 86961, Futuroscope-Chasseneuil, France*
[c] *PIMM, CNRS-ENSAM Paristech, 151 Bd de l'Hopital, 75013, Paris Cedex, France*
[d] *Institute of Polymers, Composites and Biomaterials (IPCB), National Research Council, Piazzale Enrico Fermi 1, Località Granatello, 80055, Portici (NA), Italy*

ARTICLE INFO

ABSTRACT

Polymer composite materials provide good strength to weight ratio and tailored mechanical properties thanks to the reinforcing fibres. Until recently, the need for taking into account the whole life cycle of a composite structure was neglected and only the service aspects were important. Today, the designers of a new composite structure have to take into account the environmental aspects from the sustainability of raw materials to the management of end life products. There are recycling issues related to the most popular composites. A solution for the recycling issue can be sought in green composites with reinforcing fibre originating from plants. The behaviour of eco-composites, when subjected to laser or mechanical impact loadings, is not well known yet. Short fibre composites were made with spruce fibres. Another set of samples was made of flax fibres. Also a woven hemp fabric-based eco-composite was investigated. A fully synthetic woven composite was used for comparison with green composites. Mechanical impacts were performed by means of a falling dart impact testing machine. Laser impacts were made with high power laser source. Four assessment techniques were employed in order to analyse and compare impact damage. Damage detection thresholds for each material and technique were obtained.

1. Introduction

The advantages of fibre reinforced polymer (FRP) composites allow them to replace the traditional materials in many branches of industry. They are used in more and more fields such as aeronautics (aircraft fuselage and other secondary structures) [1] or astronautics (telecom satellites) [2], energy industry (wind turbine blades) [3], shipyards (in yachts and premium ships) [4], in automotive industry (frameworks, primary and secondary parts) [5], and in civil structures for strengthening purposes [6], [7].

Until recently, the need for taking into account the whole life cycle of a composite structure was neglected and only the service aspects were considered. Nowadays, it is expected that the whole life cycle of a composite structure is planned in environment-friendly manner, starting from sustainability of raw materials and ending at the management of end life products. It is expected that the new objects should emit less greenhouse gases, consume less fuel and use low carbon-

footprint materials throughout the engineering and life-time cycle. A major approach used to more efficiently use natural resources and reduce gas emission is the use of composites structures. The first step was to exploit CFRP and GFRP to replace metal alloys, but this results in issues when the structure goes out of service. To try to overcome this issue the use of green composites, which are much more sustainable, has been proposed. In automotive industry the first attempts to make "green" cars date back to 1941 when Henry Ford presented his car with plastic panels. It is said that among many other ingredients they were made of soybeans, wheat, hemp, flax and ramie. There is also a source claiming that they were made of soybean fibre in a phenolic resin with formaldehyde [8]. Nowadays this idea is returning, and a proof of concept car called 'RENEW' was designed, being inspired to environmental safeguard. It is made of three plies of woven hemp, making it lighter than cars made from fiberglass [9]. Green composites are also a good alternative to classical synthetic composites for some semi-structural applications [[10– 13]]. Composites made of fibres from plants

---
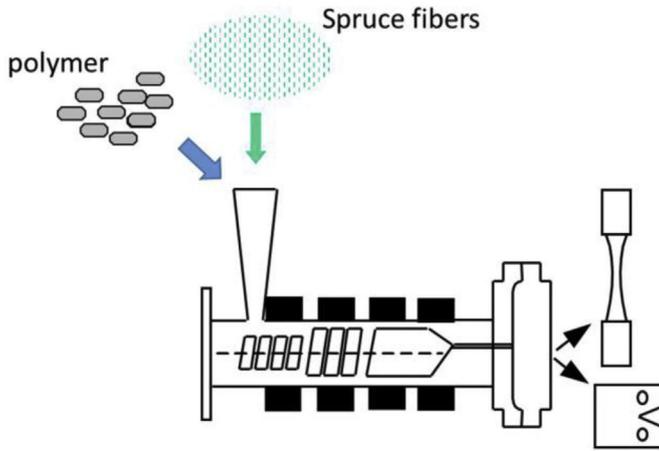
Fig. 1. Extrusion process – Twin screw extruder.
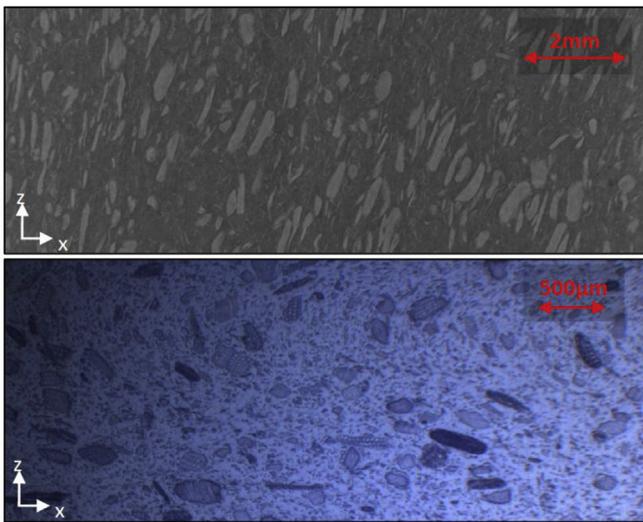

Fig. 2. Tomography of WA (up) and micrography of TWA (down).

(hemp, jute, sisal, flax, kenaf, spruce, etc.) and bio-based polymer matrices (PLA – poly(lactic acid), PHA – polyhydroxyalkanoates, etc.) are continuously investigated. Bio-based matrices have a lower carbon footprint than synthetic ones, while specific performances of natural fibres are similar to those of synthetic or mineral counterparts because of their much lower density [[14– 17]].

Albeit these promising aspects, green composites based on natural fibres still need to undergo fundamental investigations, such as high strain rate mechanical testing, to assess their capabilities and potential as conventional composites replacement. In particular, their impact behaviour received little attention. The analysis and comparison of damages induced by mechanical and laser impacts on green composites reinforced with long plant fibres was recently published [18]. The

Fig. 4. Tomography of BC3 (up) and micrography of BC4 (down).

impact-induced damage was assessed by six characterization techniques: eye observation, back face analysis, terahertz spectroscopy, laser vibrometry, x-ray micro-tomography and microscope observations. In the mentioned publication the green composites were prepared with hemp fibres and compared with a glass reinforced one [18].

The purpose of this work is to exploit such result and assessing approach to investigate the impact performance of composites reinforced with short (spruce) and medium-length (flax) fibres, and to show how such systems respond to different types of non-destructive evaluation techniques. The knowledge of the application field, sensitivity and reliability of a non-destructive technique is fundamental when the complexity of the analysed system is high, such in case of composites. For this reason, the results from two class of impact characterizations were correlated with the information provided by four assessment techniques (eye observation, back face analysis, terahertz spectroscopy and laser vibrometry) on short- and medium-length fibre reinforced systems, and compared with those from composites reinforced with long fibres (hemp and glass woven composites). Moreover, tomographic and microscope observations are presented as further information sources for the understanding of the impact behaviour of green composites.

2. Experimental

Four different eco-composites with two different fibre lengths were prepared. Due to the large number of investigated cases and because of the many different investigation methods, a selection of the possible tests was performed. This resulted in the lack of some values of mechanical impact energy or laser impact intensity tests. Short fibre samples were prepared with spruce fibres with 30% fibre content by
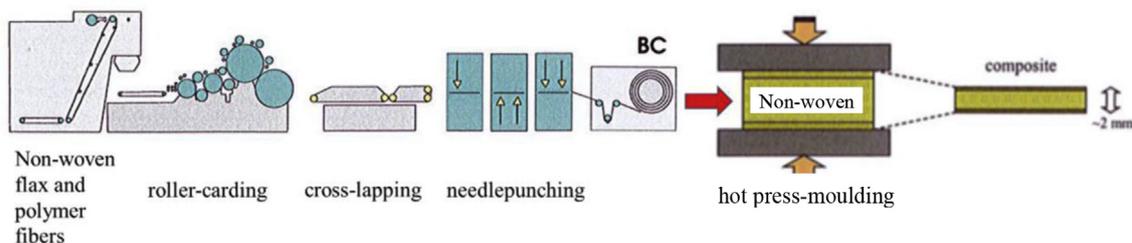

Fig. 3. Manufacturing process of BC3 and BC4.
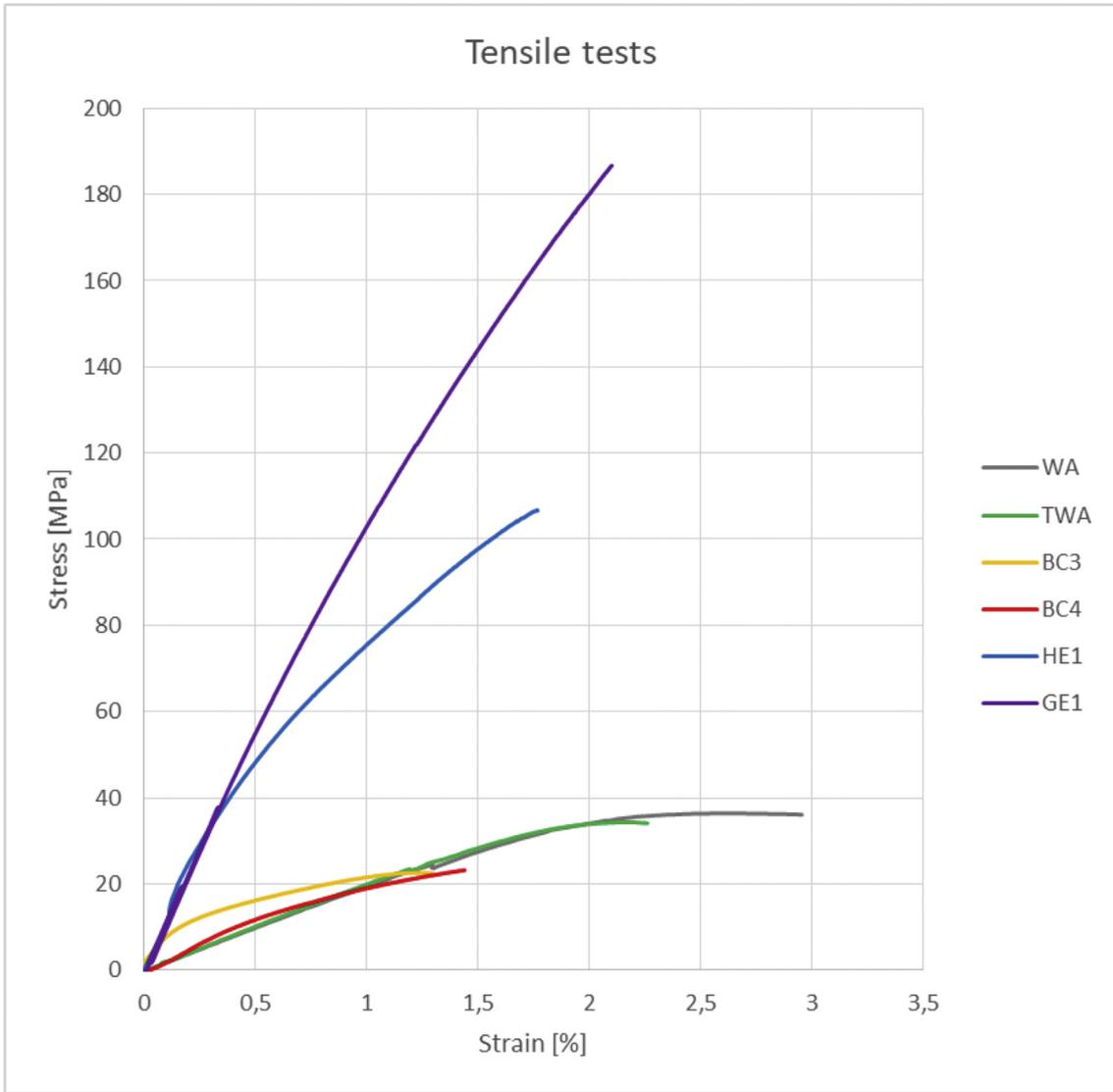
Fig. 5. Tensile test results obtained for the investigated materials.

Table 1
Values obtained from tensile tests.

	Max Stress [MPa]	Deformation at Max Stress [%]	Elastic Modulus [MPa]
WA	36.4 ± 4.7	2.62 ± 0.37	2040 ± 206
TWA	34.3 ± 4.2	2.15 ± 0.31	2080 ± 190
BC3	22.6 ± 2.5	1.22 ± 0.15	5360 ± 383
BC4	23.2 ± 2.6	1.44 ± 0.26	2720 ± 204
HE1	106.8 ± 9.5	1.77 ± 0.20	9800 ± 572
GE1	186.7 ± 12.0	2.10 ± 0.11	11440 ± 423

Fig. 6. Mechanical impact test stand.

weight in acrylo-butadiene-styrene (ABS) polymer. Spruce fibres were obtained from industrial waste, and exhibited an average length of 800 μm. These fibres were used as received for samples coded as WA and after a thermal treatment at 250 °C for samples coded as TWA. Short fibre samples were manufactured by using an injection moulding machine, which used an extruder to mix and compound the components. Plates were produced by injecting in a mould with a thickness equal to 4 mm. The process is depicted in Fig. 1. Sections of produced samples are shown in Fig. 2, where it is clearly shown the good dispersion of fibres in the polymeric matrix for both WA and TWA systems.

The medium sized fibre reinforced samples were based on flax

Fig. 7. Laser impact test stand.

Fig. 10. Back face 3D reconstruction stand.

Fig. 8. Laser induced shock wave propagation through a homogeneous material.
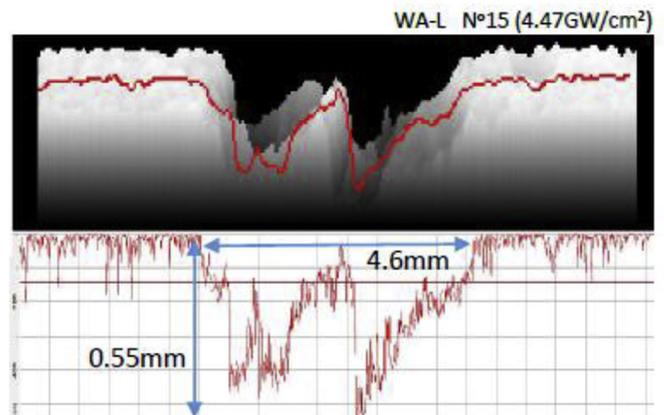
Fig. 11. 3D reconstruction and z(x) profile of laser impact on WA-L sample with 4.47 GW/cm^2 intensity.

fibres. They were coded as BC3 and BC4. Flax fibres had 60 mm length and the target fibre content by weight was 70%. Two types of thermoplastic polymers were used as matrices: polypropylene (PP), used as a reference from synthetic materials, for BC3 series and polylactide (PLA), a biodegradable polymer derived from renewable resources, for BC4 series. The manufacturing process of BC samples is depicted in Fig. 3, and it is basically a compression moulding fibre impregnation process. The final plate thickness achieved was 2 mm. The fibre dispersion and impregnation was very good, as shown in Fig. 4 for BC3 and BC4 systems.

Composites reinforced with short and medium size fibres were compared with long fibre ones. A complete investigation of long fibre reinforced composites was reported in a previous work [18], but for the sake of comparison it is worth to recall that the a) sample coded as HE1 is a composite made of 7 plies of plain woven hemp fabric (fibres were twisted with a mean angle equal to 11°, 267 $\pm$ 1 g/m^2) impregnated with epoxy resin EPOLAM 2020 from Axson Technologies., and b) the sample coded as GE1 is made of 7 plies of plain woven glass fabric impregnated with the same resin (EPOLAM 2020). HE1 and GE1 samples were prepared by vacuum infusion process to obtain plates with 4 and 2 mm thickness, respectively.

2.1. Mechanical characterization

The tensile behaviour was evaluated by means of a universal testing

Fig. 9. Backface of BC3 sample impacted mechanically at 5J (a) and by laser at 4.45 GW/cm^2.
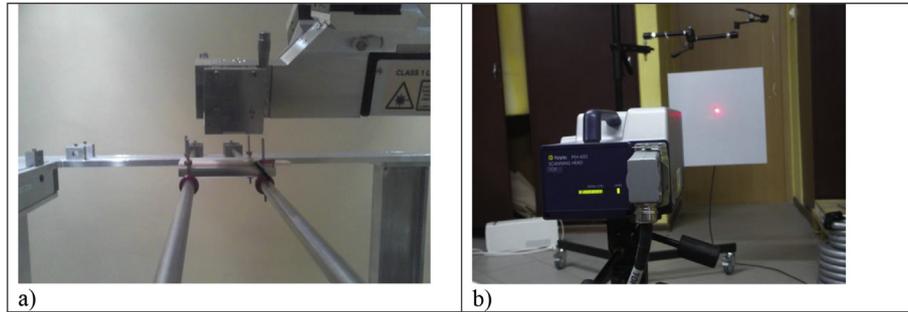
Fig. 12. Terahertz receiver and detector over a clamped sample (a); vibrometer scanning head with laser pointing at sample.
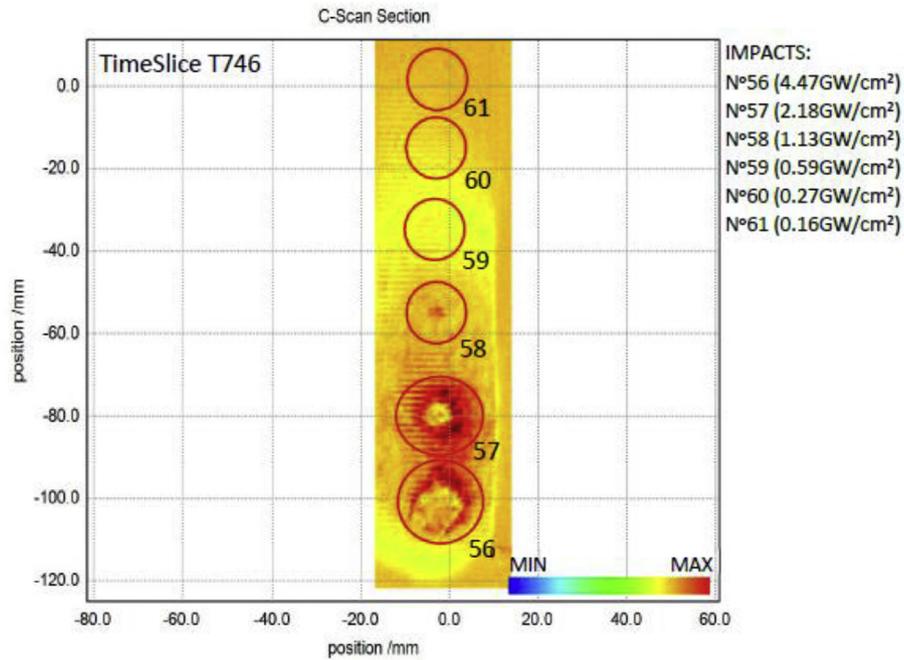
Fig. 13. C-Scan section of BC4-L sample obtained with terahertz spectroscopy.
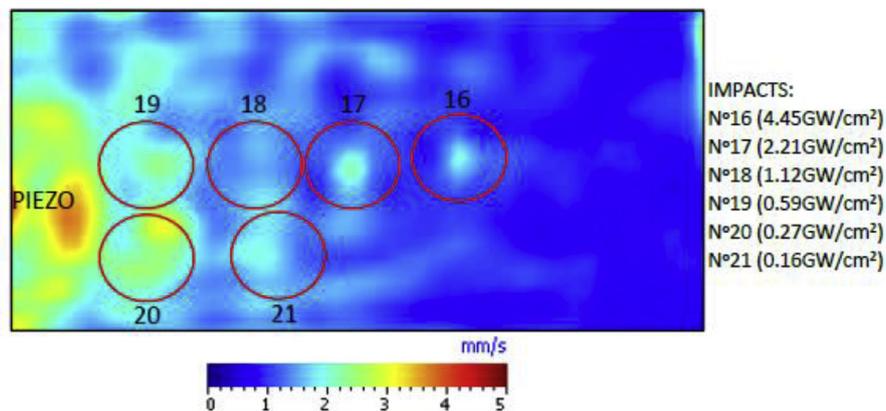
Fig. 14. RMS values obtained with laser vibrometer for TWA-L sample after laser impacts. Wave frequency f = 200 kHz.

machine (electromechanical, Instron 4505, USA) equipped with a 100 kN load cell, according to the ASTM D638 standard and the results are shown in Fig. 5. At least 3 samples of each material were tested. Average maximum stress, deformation at maximum stress and elastic modulus values are reported in Table 1. It is evident that the best performing system was based on glass fibres, followed by that based on hemp fibres. As expected, the short fibre reinforced systems were the lowest performing systems, with no apparent difference between

systems based on treated or untreated fibres, with the exception of the strain at break, higher for the non-treated samples.

2.2. Impact characterization

The investigated samples were impacted by either a falling dart (Fig. 6) and a laser beam (Fig. 7). The mechanical impacts were performed at a velocity below 2 m/s to simulate the typical impact on

Table 2
Summary of mechanical impact tests performed on the samples and techniques used for assessment of the impacts influence.

Sample	Impact energy	Eye observation	Back face relief	Terhertz spectroscopy	Vibrometry
WA-M	1.00 J	X		X	X
	2.50 J	X		X	X
	3.50 J	X		X	X
	5.00 J	X		X	X
TWA-M	1.00 J	X			X
	1.50 J	X		X	X
	2.50 J	X			X
	5.00 J	X		X	X
BC3-M	1.00 J	X	X	X	X
	1.50 J	X	X	X	X
	2.50 J	X	X	X	X
BC4-M	1.00 J	X	X	X	X
	1.50 J	X	X	X	X
	2.50 J	X		X	X
HE1-M	1.00 J	X		X	X
	2.50 J	X	X	X	X
	5.00 J	X	X	X	X
GE1-M	1.00 J	X		X	X
	2.50 J	X	X	X	X
	5.00 J	X	X	X	X

Table 3
Summary of laser impact tests performed on the samples and techniques used for assessment of the impacts influence.

Sample	Impact level	Eye observation	Back face relief	Terhertz spectroscopy	Vibrometry
WA-L	0.16 GW/cm^2	X		X	X
	0.27 GW/cm^2	X		X	X
	0.59 GW/cm^2	X		X	X
	1.13 GW/cm^2	X		X	X
	2.19 GW/cm^2	X	X	X	X
	4.47 GW/cm^2	X	X	X	X
TWA-L	0.16 GW/cm^2	X		X	X
	0.27 GW/cm^2	X		X	X
	0.59 GW/cm^2	X		**X**	**X**
	1.12 GW/cm^2	X	X	X	X
	2.21 GW/cm^2	X		X	X
	4.45 GW/cm^2	X	X	X	X
BC3-L	0.16 GW/cm^2	X		X	X
	0.27 GW/cm^2	X		X	X
	0.59 GW/cm^2	X		X	X
	1.13 GW/cm^2	X	X	X	X
	2.18 GW/cm^2	X	X	X	X
	4.45 GW/cm^2	X	X	X	X
BC4-L	0.16 GW/cm^2	X		X	X
	0.27 GW/cm^2	X		X	X
	0.59 GW/cm^2	X	X	X	X
	1.13 GW/cm^2	X	X	X	X
	2.18 GW/cm^2	X		X	X
	4.47 GW/cm^2	X	X	X	X
HE1-L	0.16 GW/cm^2	X		X	X
	0.27 GW/cm^2	X		X	X
	0.59 GW/cm^2	X		X	X
	1.15 GW/cm^2	X		X	X
	2.24 GW/cm^2	X	X	X	X
	4.46 GW/cm^2	X	X	X	X
GE1-L	0.16 GW/cm^2	X		X	X
	0.27 GW/cm^2	X		X	X
	0.60 GW/cm^2	X		X	X
	1.15 GW/cm^2	X		X	X
	2.25 GW/cm^2	X		X	X
	4.55 GW/cm^2	X	X	X	X

materials under service conditions, such as tool drops, bird strikes, hailstone damage and contact with other materials [19]. Impact tests were performed by using a falling dart impact testing machine model Fractovis Plus from CEAST (Pianezza - TO, Italy). The specimens were tested at energies in the range from 1 to 5J. The falling dart mass was constant (1.9265 kg), and the impact energy was changed by changing the impact height. The impact head was hemispherical, 12.7 mm in diameter. Samples damaged with mechanical impacts are coded with an additional 'M' (WA-M, TWA-M, BC3-M, etc.). The laser impact (laser shock) technique is a method that allows to achieve high levels of load inside the materials. It can be used for damage threshold analyses and allows, for example, the simulation of space debris and meteoroids impacts [20], assessment of adhesive bonds quality [21], or fibre/matrix interface study [22]. The laser beam causes the sublimation of the matter on sample surface, and the plasma created induces a reaction force in the form of a pressure shock wave that propagates through the material, thus applying a high tensile loading state (Fig. 8). All the samples were tested at six different laser shock intensities, keeping constant the shock beam diameter (6 mm) and the pulse duration (10.2 ns). Samples tested by the laser are coded with an additional 'L' (WA-L, TWA-L, BC3-L, etc.). Representative samples after each type of impact testing are reported in Fig. 9.

3. Damage assessment methods

Eye observation, back face relief, terahertz spectroscopy, and laser vibrometry were used in order to assess the mechanical and the laser induced damages, and their results were compared.

Back face relief was performed by means of a multidimensional image acquisition setup (Axio Imager Vario Z2 microscope from Zeiss - Germany) (Fig. 10). The dedicated softwares images for a range of equally spaced focus positions, allowing imaging of rough surfaces and 3D reconstructions. This method allows to characterize superficial damage, in particular the depth and geometry. Multidimensional images for selected impacts were captured in order to visualize the 3D surface profiles of the back face damage. A typical result of this analysis is shown in Fig. 11, where the acquisition after a laser impact at 4.47 GW/cm^2 is presented.

Terahertz spectroscopy was used because polymer composites made out of electrically not conducting materials can be analysed by using electromagnetic radiations in the terahertz frequency range. Terahertz spectroscopy technique in the time domain (THz-TDS) proved to be a suitable method for the detection of internal defects like delamination in composite materials [23], [24]. According to [25] delaminations and moisture contamination can be visualized using TDS terahertz spectroscopy but the effectiveness depends on depth, matrix material, and size of the defect. The terahertz spectrometer used was TPS Spectra 3000 from Teraview (Cambridge, United Kingdom) with radiation in the 0.1–3 THz range. The spectrometer is equipped with a moving table to apply x-y movements and scan large objects (Fig. 12a). The scanning heads operated in both reflection and transmission modes [23] [24].The C-scan of a representative sample is depicted in Fig. 13. The sample was impacted with laser at 6 locations, and the most intense damaged locations can clearly be identified (no. 56, 57 and 58).

The last investigation method is based on the analysis of propagating guided elastic waves. Guided wave propagation is a very attractive technique that can be used either in structural health monitoring (SHM) or non-destructive testing (NDT). The basis of this method is the analysis of changes in the wave propagation caused by the presence of damages because guided waves propagating in a structure interact with any discontinuities encountered. These interactions can be observed as wave reflection, scattering, diffraction or mode conversion. Many research papers report on the application of this method for the detection and localization of simulated (notch, cut, hole) or real (cracks) damages [26]. The elastic waves are sensed using a Scanning Laser Doppler Vibrometer (SLDV, PSV–400–3D, Polytec GmbH, Waldbronn, Germany) equipped with a single scanning head (Fig. 12b). In order to excite the samples a piezoelectric disc glued on inspected samples was used (0.5 mm-thick and 10 mm in diameter). The
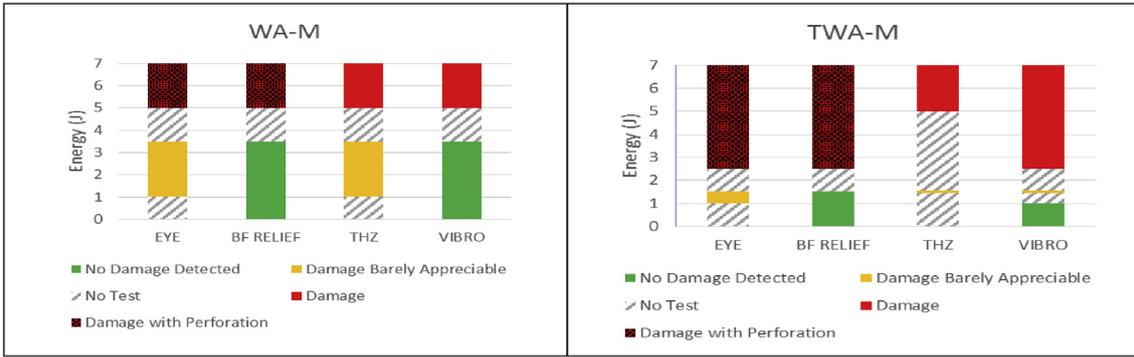
**Fig. 15.** Damage detection thresholds of WA-M and TWA-M samples.
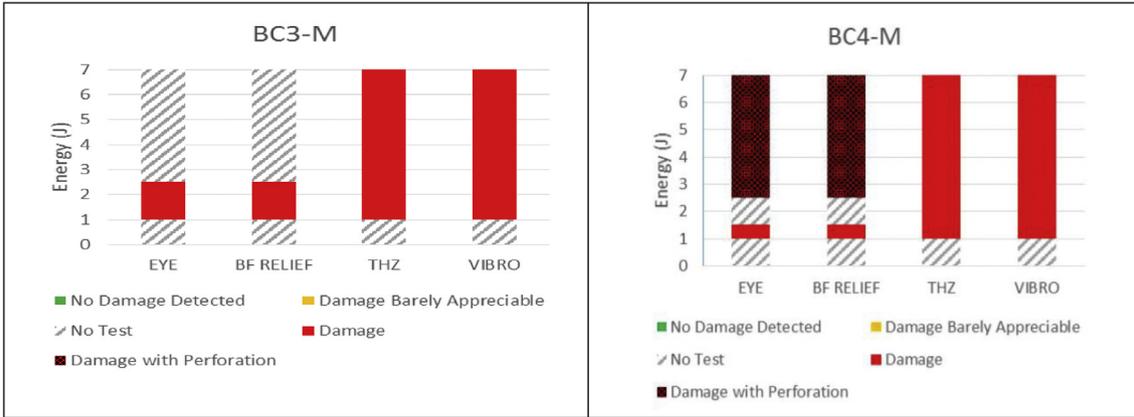
Fig. 16. Damage detection thresholds of BC3-M and BC4-M samples.
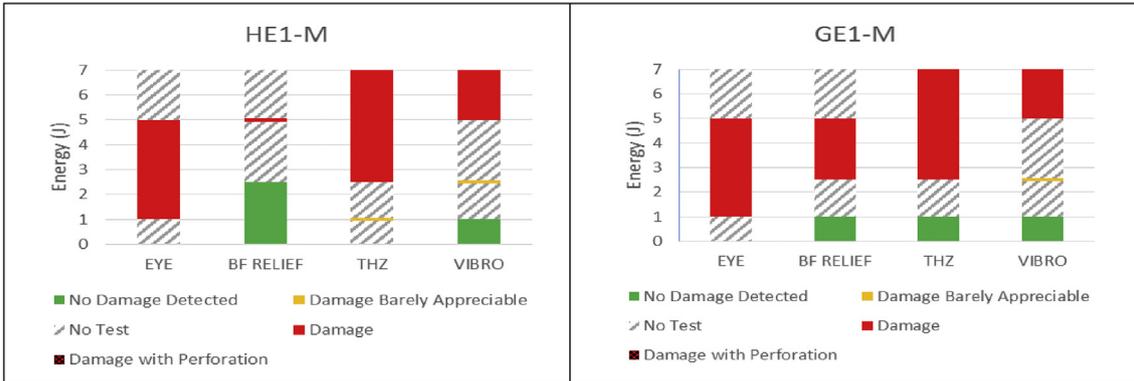

Fig. 17. Damage detection thresholds of HE1-M and GE1-M samples.

analysis of the results was based on a well-established procedure that calculates the root mean square (RMS) value for each point [27]. RMS values are different in damaged and non-damaged regions because guided elastic waves are altered at damage location [28]. The RMS result obtained for TWA-L sample is presented in Fig. 14. The sample was impacted at 6 locations with laser. Depending on the intensity of the laser there is a different RMS detected level. The RMS level is also influenced by the position of the damage with respect to the piezo-electric transducer (PIEZO). The elastic wave going from the transducer to damage location no. 16 has to travel through areas where other damage is present. This causes wave scattering and influences the RMS wave energy detected at the location of damage.

4. Results and discussion

The details regarding the falling dart tests are presented in Table 2.

The samples are listed together with impact energy and assessment method used for each case. A selection of samples was performed. The result was that two impact cases (namely TWA-M at 1.00 and 2.5 J) were not investigated by means of Terahertz Spectroscopy, while a selection of impact conditions (all BC3-M cases and partially BC4-M, HE1-M and GE1-M cases) were analysed with Back Face Relief. Analogous information is provided in Table 3 for laser impacted samples. More impact levels were considered in this scenario and only Back Face Relief analysis was not performed for all the samples. It is important to notice that intensity levels can slightly differ between samples. For example, WA-L sample was impacted at 4.47 GW/cm^2 and TWA-L sample at 4.45 GW/cm^2. There are various other examples like this in Table 3. The reason is due to the fact that these values are the actual measurements at the equipment output and hence are not calculations based on parameters set before the test.

Due to the large amount of data gathered (two types of impact,

Table 4
Minimal detected damaged areas for dart impacts.

Sample	Method	Clearly detected impact level [J]	Damaged area on front face [mm²]	Damaged area on back face [mm²]
WA-M	Eye obs.	5.00	140	580
	Back face relief	5.00	140	580
	Terahertz spectroscopy	5.00	140	580
	Vibrometry	5.00	140	580
TWA-M	Eye obs.	2.50	90	800
	Back face relief	2.50	90	800
	Terahertz spectroscopy	5.00	130	800
	Vibrometry	2.50	90	800
BC3-M	Eye obs.	1.00	40	100
	Back face relief	1.00	40	100
	Terahertz spectroscopy	1.00	40	100
	Vibrometry	1.00	40	100
BC4-M	Eye obs.	1.00	110	127
	Back face relief	1.00	110	127
	Terahertz spectroscopy	1.00	110	127
	Vibrometry	1.00	110	127
HE1-M	Eye obs.	1.00	25	127
	Back face relief	5.00	90	550
	Terahertz spectroscopy	2.50	60	420
	Vibrometry	5.00	90	550
GE1-M	Eye obs.	1.00	20	20
	Back face relief	2.50	30	40
	Terahertz spectroscopy	2.50	30	40
	Vibrometry	5.00	70	80

various impact levels, four assessment methods, six types of samples) results are presented as bar plots with energy or intensity levels on the vertical axis and type of assessment method on the horizontal one. A colour coding was used to indicate the result of assessment. Green colour means that no damages were observed. Orange colour indicates a barely visible damage, light red represents a clear damage, while dark red indicates perforation (mechanical impact) or spallation (laser impact). To limit the number of experiments, mechanical and laser impacts were performed at selected values of energy or intensity, respectively. So, for some values of energy or intensity no data are available.

4.1. Falling dart impacts

In systems reinforced with short fibres (WA-M and TWA-M), the occurrence of damaging was clearly detected after a mechanical impact at 5 J for WA-M and 2.5 J for TWA-M (Fig. 15). Both eye observation and back face relief clearly detected the perforation. The terahertz spectroscopy and vibrometry were not able to detect the perforation and only light damage was shown (marked as light red). Eye observation and THz-TDS techniques were more sensitive than the other two in the detection of damage initiation after an impact at 1.0 J.

The results for samples with medium-length fibres (BC3-M and BC4-M) are depicted in Fig. 16. Damaging was observed already after the impact at 1.0 J and the damage threshold for BC4-M was as for TWA-M sample (Fig. 15), since already after an impact at 2.5 J perforation was detected.

Long fibre samples after mechanical impacts (HE1-M and GE1-M) presented a different behaviour (Fig. 17) because in none of the cases perforation was observed, as expected due to the much higher strength of the composites. On the contrary, eye observation indicated clear damage presence already at 1.0 J. The initiation of damage was also observed with the terahertz spectroscopy but only for the sample reinforced with hemp fabric (HE1-M).

After determining the damage thresholds it was possible to determine the damage size for each sample and each technique. The measured damaged areas on front and back faces are reported in Table 4. It should be noted that only cases that gave clear indication of damage in Fig. 15–17 were considered for being reported. Damage area is higher with higher impact level. In addition, the areas on back surfaces are bigger than on front surfaces.

4.2. Laser impacts

The results for laser impacts on samples with short fibres are presented in Fig. 18. The initiation of damage was observed already below 1 GW/cm² using the terahertz-based method in WA-L while in the case of TWA-L no damage was observed by any of the analysis methods after the impact at 1 GW/cm².

Damages below 1 GW/cm² were also observed for medium-length samples (Fig. 19). None of the samples experienced spallation for the considered test cases. But it should be noticed that only the terahertz and vibrometry techniques were tested for impacts up to 7 GW/cm², while eye observation and back face relief analyses were performed up to 4.5 GW/cm².

In long fibre samples impacted by the laser technique a clear spallation was observed for the hemp reinforced sample above 4 GW/cm² (Fig. 20). Eye observation allowed to detect a lower damage threshold for the 'green' composite (HE1-L) with respect to the fully synthetic one (GE1-L) since the initiation of damage appeared below 1 GW/cm².

After determining the damage thresholds for laser impacts it was possible to estimate the damage size for each sample and each technique. The measured damaged areas on back faces are reported in Table 5. It should be noted that only cases that gave clear indication of damage according to Fig. 18–20 were considered for being reported.
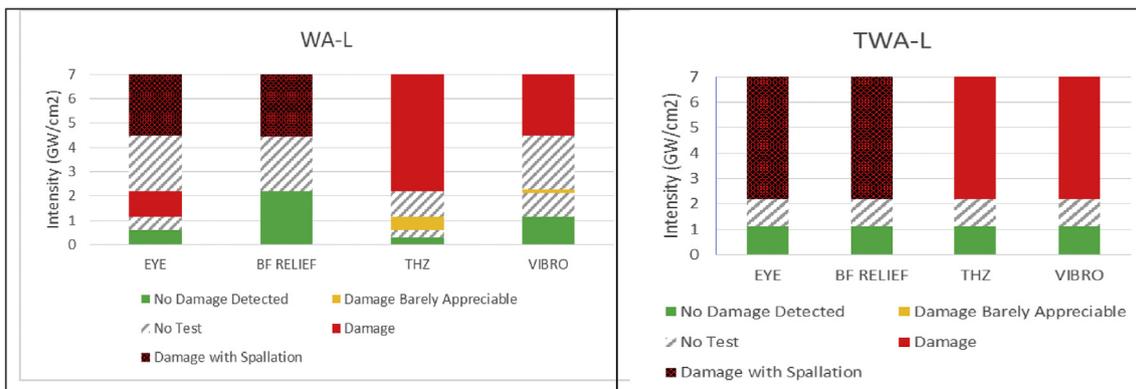

**Fig. 18.** Damage detection thresholds of WA-L and TWA-L samples.
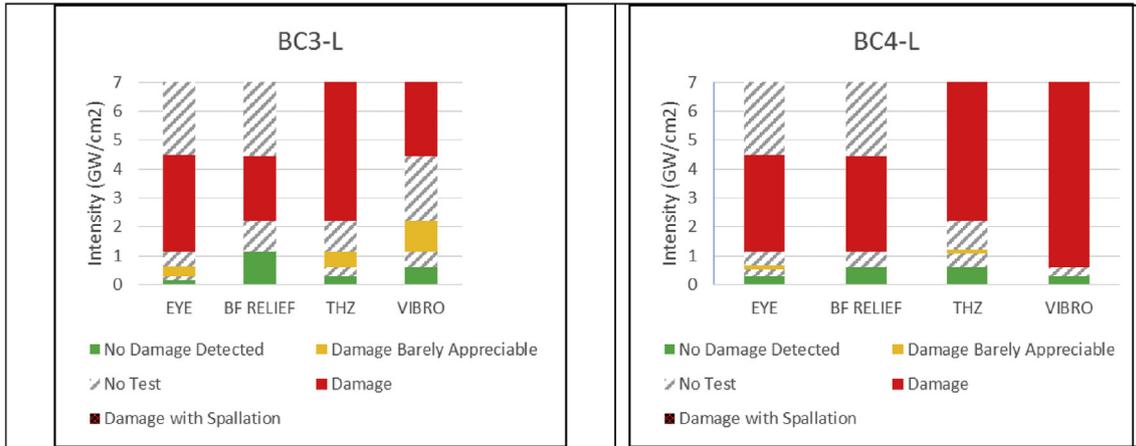
**Fig. 19.** Damage detection thresholds of BC3-L and BC4-L samples.
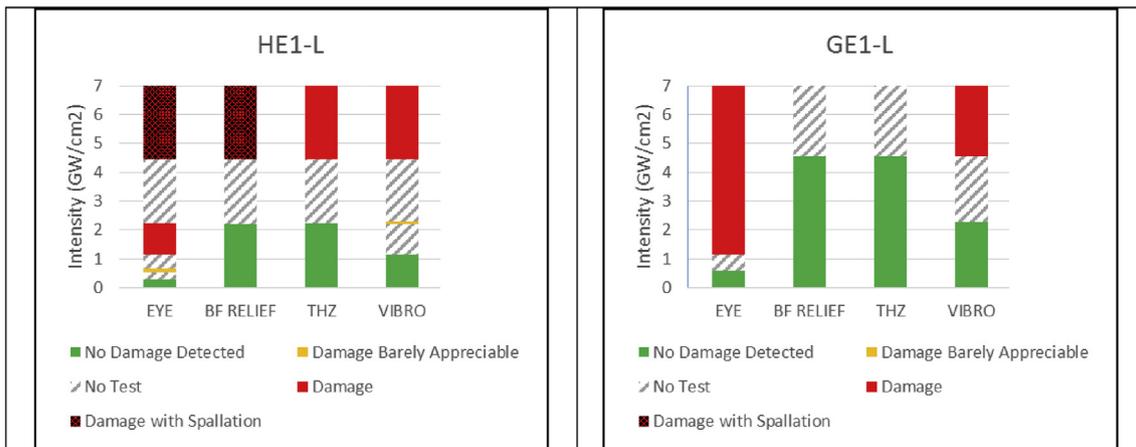
Fig. 20. Damage detection thresholds of HE1-L and GE1-L samples.

Table 5
Minimal detected damaged areas for laser impacts.

| Sample	Method	Clearly detected impact level [G/cm²]	Damaged area on back face [mm²]
WA-L	Eye obs.	1.13	8
	Back face relief	4.47	22
	Terahertz spectroscopy	2.19	13
	Vibrometry	4.47	22
TWA-L	Eye obs.	2.21	10
	Back face relief	2.21	10
	Terahertz spectroscopy	2.21	10
	Vibrometry	2.21	10
BC3-L	Eye obs.	1.13	8
	Back face relief	2.18	16
	Terahertz spectroscopy	2.18	16
	Vibrometry	4.45	44
BC4-L	Eye obs.	1.13	8
	Back face relief	1.13	8
	Terahertz spectroscopy	2.18	20
	Vibrometry	0.59	3
HE1-L	Eye obs.	1.15	12
	Back face relief	4.46	38
	Terahertz spectroscopy	4.46	38
	Vibrometry	4.46	38
GE1-L	Eye obs.	1.15	8
	Vibrometry	4.55	38
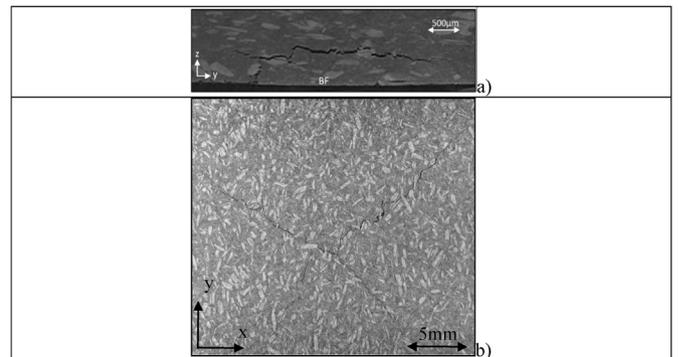
Fig. 21. X-ray micro-computed tomography for a) WA-L sample impacted at 2.19 GW/cm², b) WA-M sample impacted at 2.5J.

Damage area is higher with higher impact level.

4.3. Tomography and microscopic observations

The four assessment methods provided relevant information about the damage threshold in the different systems. Tomography and microscopy were used as secondary auxiliary methods of observation to analyse selected cases to better detect and asses the damaging.

X-ray micro-tomography is a well-established technique that provides reconstruction of three-dimensional volumes from a sequence of projection images taken at different angles while the material is turned

Fig. 22. X-ray micro-computed tomography for BC3-M sample impacted at 1J.
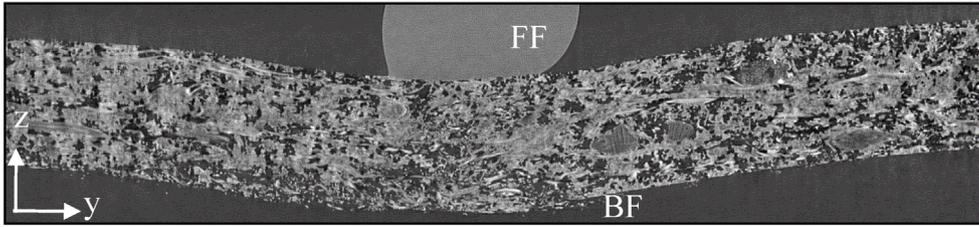
along a rotation axis [29]. The result of the reconstruction process is a series of images at different consecutive sections along each orthogonal axis. Image acquisition has been performed using an UltraTom CT scanner manufactured by RX Solutions (France) with 12 μm resolution. An example of tomographic image is presented in Fig. 21, from the WA-L dataset. The second auxiliary method of observation was based on the Reichert-Jung optical microscope. Samples had to be accurately prepared to allow the correct detection of fine details hence they were carefully cut and prepared, in order to avoid contamination and the development of new damage. After the cutting, samples were embedded into a resin to improve their grip during polishing. Finally, surfaces of specimens were polished and then underwent the optical microscopy observation.

Systems reinforced with short and medium length fibres already showed clear damages after the impact at 1 J. A cross-shaped damage is visible in the z-plane of the WA-M tomographic image (Fig. 21b), while in the x-plane some cracks are visible, propagating through matrix and fibres up to the back face. Tomographs in x-plane of BC3-M at 1J showed large deformation induced by the mechanical impact (Fig. 22). The deformation of BC3-M was confirmed by the microscope observations, as well as for BC4-M impacted at 1J. In addition, areas near the back face presenting debonding at the fibre-matrix interface were also detected.

The tomography for the HE1-M sample impacted at 2.5J showed the typical cross shaped damaging in z-plane, representing the preferential directions, along 0° and 90°, for damage propagation. In the x-plane a conical pattern was detected in the thickness [30] [31], showing the increasing damage from the impacted front face towards the back face. This damage is related to matrix cracking and debonding at the fibre-matrix interface and to the propagation through the thickness. Furthermore, a possible fibre failure near back face is observed. GE1-M sample impacted at 2.5J presents clear damaging near the back face (fibre breakage and matrix cracks are observed in the z-plane), while microscope observations for 1J impact showed some areas with cracks at the fibre-matrix interface and delaminations. No damage was detected near the back face.

In regard to laser impacts, the tomographic analysis of the WA-L system impacted at 2.19 GW/cm^2 showed damaging near the back face (Fig. 21a). In particular, cracks propagating through matrix and fibres were detected. Tomographs of samples impacted at lower laser intensities (0.27, 0.59 and 1.13 GW/cm^2) didn't show any damage. Micrographs of TWA-L impacted at 2.19 GW/cm^2 showed a similar behaviour with respect to WA-L, hence cracks propagated through both matrix and fibres. However, quantitatively TWA-L presents more serious damage, because the cracks were longer and the sample was close to spallation. Impacts on medium fibre length composites showed different degrees of deformation. For example, the BC4-L internal damage after the 2.18 GW/cm^2 impact showed a similar damage with respect to the mechanical impacts, presenting areas with debonding at the fibre-matrix interface. HE1-L was analysed after 2.24 GW/cm^2 and 4.46 GW/cm^2 impacts. Matrix cracks and cracks at the yarn-matrix interface were observed near the back face in the first case, while spallation and fibre failure additionally occurred after the higher energy impact, as clearly evidenced by the tomographic analysis. Tomographs of GE1-L did not show any damage after impacts at several intensities (0.60, 1.15, 2.25, 4.55 GW/cm^2). However, the microscope observation for 4.55 GW/cm^2

was able to show the occurrence of debonding at the fibres-matrix interface and delamination.

5. Conclusions

The aim of the paper was to study the effect of impacts on plant fibre-based composites and to show the sensitivity of different assessment techniques in detecting the damage induced by low energy mechanical impacts or laser shock ones. The different damage evaluation techniques were used to estimate the actual damage after each impact. Two classes of impacts were applied on the composites and their damage thresholds were estimated. In general eye observation and terahertz techniques allowed to detect damages at an earlier stage with respect to back face relief and vibrometry in case of mechanical impacts, hence lower energies were needed to detect a damage. Among the investigations techniques, eye observation was the most sensitive, allowing to detect induced defects in the best performing laminate (GE1-M) after an impact at 1J (a white-coloured area is visible through back and front surfaces). In composites made of medium length fibres, namely BC3-M and BC4-M systems, damages were detected with all the techniques.

Also in case of laser impacts, eye observation proved to be the most sensitive, and damages at low intensities were correctly detected. Together with eye observation, the terahertz technique for WA-L and BC3-L samples, and vibrometry for BC4-L sample detected the low intensity damage caused by the impact of a laser beam with an intensity lower than 1.00 GW/cm^2. Even if eye observation, back face relief, terahertz spectroscopy and vibrometry all allow to detect and roughly locate the damage, they do not present enough precision to infer on damage mechanisms. For this purpose, X-ray micro-tomography and microscope observations are most suitable. Damage induced by mechanical and laser impacts shows relevant differences. In laser impacted samples, the induced damage is located near the back face. However, in mechanically impacted samples damage appears close to the front face and propagates towards the back face. Albeit damaging was developed in different positions, the main damage mechanisms are similar for each system. In fact, both mechanical and laser impacts induce in WA and TWA cracks propagating through matrix and fibres, in BC3 and BC4 deformation and debonding at the fibres-matrix interface, and in HE1 and GE1 matrix cracks, fibre failure, debonding at the fibres-matrix interface and delamination.

Damage shape on back surfaces is different after mechanical or laser impacts for short, medium and long fibre composites. For example, mechanical impacts induce cross-shaped damage in WA and TWA, while laser impacts show discoloured circular areas. For HE1 and GE1, both mechanical and laser impacts show white circular areas denoting internal damage. Only HE1-M presented additional cross-shaped damaging propagating in the fibres plane. Obtained results may serve as a useful baseline for designing structures out of investigated plant fibre-based composites.

Acknowledgments

References

[1] Guermazi N, Tarjem AB, Ksouri I, Ayedi HF. On the durability of FRP composites for aircraft structures in hygrothermal conditioning. Compos B Eng 2016;85:294–304.

[2] Park SY, Choi HS, Choi WJ, Kwon H. Effect of vacuum thermal cyclic exposures on unidirectional carbon fiber/epoxy composites for low earth orbit space applications. Compos B Eng 2012;43(2):726–38.

[3] Javaid Umair, Khan Zaffar M, Khan MB, Bassyouni M, Abdel-Hamid SM-S, Abdel-Aziz MH, ul Hasan Syed W. Fabrication and thermo-mechanical characterization of glass fiber/vinyl ester wind turbine rotor blade. Compos B Eng 2016;91:257–66.

[4] Rajapakse DSY, Hui D. Marine Composites and Sandwich Structures. Compos B Eng 2008;39(1):1–4.

[5] Balakrishnan Venkateswaran Santhanakrishnan, Seidlitz Holger. Potential repair techniques for automotive composites: a review. Compos B Eng 2018;145:28–38.

[6] Zhou Ao, Qin Renyuan, Feo Luciano, Penna Rosa, Lau Denvid. Investigation on interfacial defect criticality of FRP-bonded concrete beams. Compos B Eng 2017;113:80–90.

[7] Triantafyllou Garyfalia G, Rousakis Theodoros C, Karabinis Athanasios I. Corroded RC beams patch repaired and strengthened in flexure with fiber-reinforced polymer laminates. Compos B Eng 2017;112:125–36.

[8] https://www.thehenryford.org/collections-and-research/digital-resources/popular-topics/soy-bean-car/ (accessed on 3rd of July 2017).

[9] http://nypost.com/2016/05/06/this-car-is-made-out-of-cannabis-hemp/ (accessed on 3rd of July 2017).

[10] Corbiere-Nicollier T, Gfeller Laban B, Lundquist L, Leterrier Y, Månson J-AE, Jolliet O. Life cycle assessment of biofibres replacing glass fibres as reinforcement in plastics. Resour Conserv Recycl 2001;33:267–87.

[11] Joshi SV, Drzal LT, Mohanty AK, Arora S. Are natural fiber composites environmentally superior to glass fiber reinforced composites? Compos Appl Sci Manuf 2004;35(No. 3):371–6.

[12] Goutianos S, Peijs T, Nystrom B, Skrifvars M. Development of flax fibre based textile reinforcements for composite applications. Appl Compos Mater 2006;13:199–215.

[13] Faruk O, Bledzki AK, Fink H-P, Sain M. Biocomposites reinforced with natural fibers: 2000-2010. Prog Polym Sci 2012;37:1552–96.

[14] Wambua P, Ivens J, Verpoest I. Natural fibres: can they replace glass in fibre reinforced plastics? Compos Sci Technol 2003;63(No. 9):1259–64.

[15] Vasconcellos D, Sarasini F, Touchard F, Chocinski-Arnault L, Pucci M, Santulli C, Tirillò J, Iannace S, Sorrentino L. Influence of low velocity impact on fatigue behaviour of woven hemp fibre reinforced epoxy composites. Composites Part B 2014;66:46–57.

[16] Vasconcellos D, Touchard F, Chocinski-Arnault L. Tension-tension fatigue behaviour of woven hemp fibre reinforced epoxy composite: a multi-instrumented damage analysis. Int J Fatig 2014;59:159–69.

[17] Perrier A, Touchard F, Chocinski-Arnault L, Mellier D. Mechanical behaviour analysis of the interface in single hemp yarn composites: DIC measurements and FEM calculations. Polym Test 2016;52:1–8.

[18] Touchard F, Boustie M, Chocinski-Arnault L, Pascual González P, Berthe L, Vasconcellos D, Sorrentino L, Malinowski P, Ostachowicz W. Mechanical and laser impact effects on woven composites with hemp or glass fibres. Int J Struct Integr 2017;8(3):1–24.

[19] Mathivanan NR, Jerald J. Experimental investigation of low-velocity impact characteristics of woven glass fiber epoxy matrix composite laminates of EP3 grade. Mater Des 2010;31:4553–60.

[20] Katz S, Grossman E, Gouzman I, Murat M, Wiesel E, Wagner HD. Response of composite materials to hypervelocity impact. Int J Impact Eng 2008;35:1606–11.

[21] Ecault R, Touchard F, Boustie M, Berthe L, Dominguez N. Numerical modeling of laser-induced shock experiments for the development of the adhesion test for bonded composite materials. Compos Struct 2016;152:382–94.

[22] Perrier A, Ecault R, Touchard F, Vidal Urriza M, Baillargeat J, Chocinski-Arnault L, Boustie M. Towards the development of laser shock test for mechanical characterisation of fibre/matrix interface in eco-composite. Polym Test 2015;44:125–34.

[23] Kuei-Hsu D, Lee K-S, Park JW, Woo Y-D, Im K-H. NDE inspection of terahertz waves in wind turbine composites. Int J Precis Eng Manuf 2012;13(7):1183–9.

[24] Im K-H, Kuei-Hsu D, Chiou C-P, et al. Terahertz wave approach and application on FRP composites. Adv Mater Sci Eng 2013;2013:563962https://doi.org/10.1155/2013/563962. 10 pages.

[25] Ospald F, Zouaghi W, Beigang R, et al. Aeronautics composite material inspection with a terahertz time-domain spectroscopy system. Opt Eng 2013;000153(3):031208.

[26] Giurgiutiu V. Structural Health Monitoring with piezoelectric wafer active sensors. Elsevier; 2008.

[27] Radzieński M, Doliński Ł, Krawczuk M, Żak A, Ostachowicz W. Application of RMS for damage detection by guided elastic waves. J Phys Conf 2011;305:012085.

[28] Kudela P, Wandowski T, Malinowski P, Ostachowicz W. Application of scanning laser Doppler vibrometry for delamination detection in composite structures. Optic Laser Eng 2017;99:46–57. https://doi.org/10.1016/j.optlaseng.2016.10.022.

[29] Landis EN, Keane DT. X-ray microtomography. Mater Charact 2010;61(12):1305–16.

[30] Shyr TW, Pan YH. Impact resistance and damage characteristics of composite laminates. Compos Struct 2003;62:193–203.

[31] Petit S, Bouvet C, Bergerot A, Barrau J. Impact and compression after impact experimental study of a composite laminate with a cork thermal shield. Compos Sci Technol 2007;67:3286–99.